

Negative thermal expansion and itinerant ferromagnetism in $\text{Mn}_{1.4}\text{Fe}_{3.6}\text{Si}_3$

Vikram Singh* and R. Nath†

School of Physics, Indian Institute of Science Education and Research Thiruvananthapuram-695551, India

(Dated: February 11, 2022)

We report the thermal expansion, critical behavior, magnetocaloric effect (MCE), and magnetoresistance (MR) on the polycrystalline $\text{Mn}_{1.4}\text{Fe}_{3.6}\text{Si}_3$ compound around the ferromagnetic transition. A large negative volume thermal expansion ($\alpha_V \sim -20 \times 10^{-6} \text{ K}^{-1}$) is observed across the transition temperature with a strong anisotropic variation of lattice parameters in the ab -plane. The anisotropic magnetoelasticity arises from the competition between magnetic ordering and structural deformation which could be responsible for the large MCE ($\Delta S_m \simeq -6 \text{ J/Kg-K}$) across the magnetic transition in this compound. The large and negative MR ($\sim -3\%$ in 80 kOe) is also observed at the transition temperature which can be attributed to the suppression of spin disorder. Further, the Rhodes-Wolfarth ratio ($RWR > 1$) and identical field dependence of MR and MCE isotherms indicate the itinerant character of the $3d$ electrons. The critical exponents determined from the analysis of magnetization and MCE are consistent with the quasi-two-dimensional (2D) Ising model with long range exchange interactions which decays as $J(r) \sim r^{-3.41}$. This unconventional quasi-2D Ising character with long-range interactions can be ascribed to strong ab -plane anisotropy and the delocalized $3d$ electrons in the studied compound.

PACS numbers: 71.20.Be 71.20.Lp 77.80.Bh 75.30.Gw 75.40.Cx 75.30.Sg 75.50.Cc 65.40.De 73.43.Qt

I. INTRODUCTION

In the past decades, research on materials with almost zero thermal expansion (ZTE) and negative thermal expansion (NTE) has been significantly enhanced due to their potential technological applications [1]. Recently, the large or giant NTE has been found in a variety of materials including oxides, intermetallics, alloys, antiperovskites, fluorides, and organometallic frameworks over a wide range of temperature [2–13]. Among these materials, the NTE in compounds with large magnetocaloric effect (MCE) has attracted special attention due to strong magnetoelastic coupling. In these materials, the NTE occurs as a result of the volume expansion accompanied by magnetic transition, known as magnetovolume effect (MVE) which dominates over the conventional phononic thermal expansion [1]. Here, a disordered magnetic phase with smaller volume transforms to an ordered magnetic structure with larger volume as the temperature decreases, causing a negative thermal expansion [4]. Prominent examples include $\text{La}(\text{Fe},\text{Si})_{13}$, $\text{Tb}(\text{Co},\text{Fe})_2$, Mn_3Ge , $R_2\text{Fe}_{17}$ (R = rare earth elements), $(\text{Hf},\text{Ta})\text{Fe}_2$, $(\text{Sc},\text{Ti})\text{Fe}_2$, MnCoGe etc [8, 14–19]. Furthermore, the manipulation or control of NTE via different routes such as chemical substitution, nano-crystallization, introduction of disorder, and application of external pressure and magnetic field provides extra working flexibility and advantage in multifunctional applications in these materials.

Basically, these MCE materials are divided into two categories based on the nature of the magnetic transition: first order transition and second order transition.

In the first order, the magnetic transition is accompanied with an abrupt structural deformation which gives rise to the sharp and large MVE at the transition. The colossal NTE in such materials is mainly associated with the abrupt enhancement of unit cell volume at the transition and is being investigated extensively in the recent days [11]. On the other hand, the pronounced NTE across a continuous second order transition has been observed only in few selected MCE materials including the Invar alloys and intermetallic compounds $\text{La}(\text{Fe},\text{Co},\text{Si})_{13}$ due to the itinerant ferromagnetism and magnetoelastic coupling [1, 3, 8].

MnFe_4Si_3 undergoes a paramagnetic (PM) to ferromagnetic (FM) transition upon cooling near room temperature without altering the crystal symmetry (hexagonal) and shows large MCE around the transition. During cooling, the crystal lattice experiences an expansion along the a -axis, while the unit cell volume shows only a weak plateau across the transition temperature [20]. Subsequently, Herlitschke et al reported that MnFe_4Si_3 exhibits magnetoelasticity across the magnetic transition [21]. Similar to the other systems, one can tune/control the strength of magnetoelastic coupling in the compound under investigation by chemical substitution [22–25]. Therefore, it would be interesting to investigate the thermal expansion behaviour of the $\text{Mn}_{1+x}\text{Fe}_{4-x}\text{Si}_3$ series along with the magnetic properties across the PM-FM transition. Recently, we have investigated the $\text{Mn}_{1+x}\text{Fe}_{4-x}\text{Si}_3$ series for $x = 0$ to 1 and found that the magnetic transition can be tuned continuously from above room temperature to lower temperatures with increasing x . A detailed analysis of magnetization and MCE for two compositions ($x = 0.0$ and 0.2) suggest that this series of compounds can be used for continuous room temperature magnetic refrigeration purpose. The critical analysis of the magnetization and MCE across

* vikram51128@gmail.com

† rnath@iisertvm.ac.in

the PM-FM transition for $x = 0$ and 0.2 yield similar but unconventional critical behavior, the origin of which is not yet clear [26]. Further, as there is a magnetoelastic coupling, one expects a correlation between thermal expansion and magnetic behaviour which was overlooked in our previous study.

In the present work, we choose another composition $x = 0.4$ ($\text{Mn}_{1.4}\text{Fe}_{3.6}\text{Si}_3$) and thoroughly investigated the thermal expansion, magnetization, magnetoresistance (MR), and critical behavior around $T_C \simeq 254$ K. Our experiments demonstrate that $\text{Mn}_{1.4}\text{Fe}_{3.6}\text{Si}_3$ exhibits a large NTE across the magnetic transition and almost ZTE below the transition. We observed that the critical behavior is not altered with varying x and the values of critical exponents are found to be similar to other itinerant ferromagnets reported in the literature. This unconventional critical behavior is explained in terms of strong anisotropy and itinerant character of the $3d$ electrons in the compound.

II. EXPERIMENTAL DETAILS

Polycrystalline sample of $\text{Mn}_{1.4}\text{Fe}_{3.6}\text{Si}_3$ is synthesized by arc melting followed by thermal annealing in vacuum at 950 °C for five days. To check the phase purity, powder x-ray diffraction (XRD) is performed using PANalytical X'Pert Pro diffractometer with Cu K_α -source ($\lambda = 1.5406$ Å). To analyze the structural changes across the magnetic transition, temperature dependent powder XRD measurements are performed in a temperature range 300 K to 15 K. For this purpose, an Oxford PheniX closed cycle helium cryostat is used as an attachment to the diffractometer. Rietveld refinement of the XRD data is performed using FullProf software package [27]. The dc - and ac - magnetic measurements as a function of temperature and magnetic field are performed using Vibrating Sample Magnetometer (VSM) and ac -susceptibility options of 9 Tesla PPMS (Quantum Design), respectively. While measuring magnetic isotherms at and below T_C , the demagnetization field has been subtracted from the applied field following the procedure described in Ref. [28]. The temperature dependent (4-300 K) resistivity is measured using four probe method in a home made resistivity set-up attached to a cryostat (M/s. OXFORD Instrument, UK) with 8 Tesla superconducting magnet. For the magnetoresistance measurement, the magnetic field is applied in the longitudinal geometry.

III. RESULTS AND DISCUSSION

A. X-ray Diffraction

Figure 1(a) and (b) present the Rietveld refinement of the powder XRD patterns of $\text{Mn}_{1.4}\text{Fe}_{3.6}\text{Si}_3$ measured at $T = 300$ K and 15 K, respectively. Both the patterns can

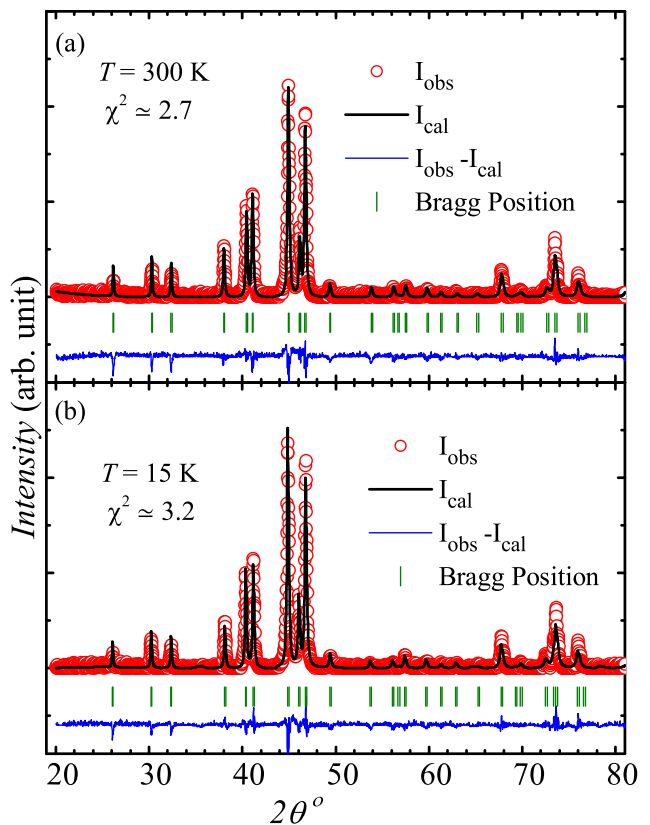


FIG. 1. The powder XRD patterns of $\text{Mn}_{1.4}\text{Fe}_{3.6}\text{Si}_3$ (a) at room temperature and (b) at $T = 15$ K. The solid black line represents the Rietveld refinement of the experimental data, the green vertical bars correspond to Bragg positions, and the bottom blue line represents the difference between observed and calculated intensities.

be refined with space group $P6_3/mcm$ of the hexagonal crystal symmetry, without detecting any extra peak. The lattice parameters [$a = 6.8112(4)$ Å, $c = 4.7351(3)$ Å, and unit cell volume $V = 190.06(2)$ Å³] obtained from the refinement of the room temperature XRD are in good agreement with our previous report [26].

The variation of lattice parameters (a , c , and V) as a function of temperature is shown in Fig. 2. As the temperature is lowered from 300 K, a remains almost constant down to ~ 270 K and then exhibits a continuous rise below 270 K, the temperature below which the PM to FM transition sets in. In contrast, c decreases monotonically from 300 K without showing any clear anomaly at the transition temperature. The overall unit cell volume features a sharp dip at the transition temperature. This indicates a strong coupling of lattice deformation in the ab -plane with the magnetization or magnetic transition.

Further, to explore the relation between the lattice expansion and magnetism, we have extracted the thermal expansion co-efficients $\alpha_A = \frac{1}{A} \left(\frac{\partial A}{\partial T} \right)_P$, where A stands for the lattice parameters (a , c , and V) and P is the pressure. The obtained thermal expansion co-efficients

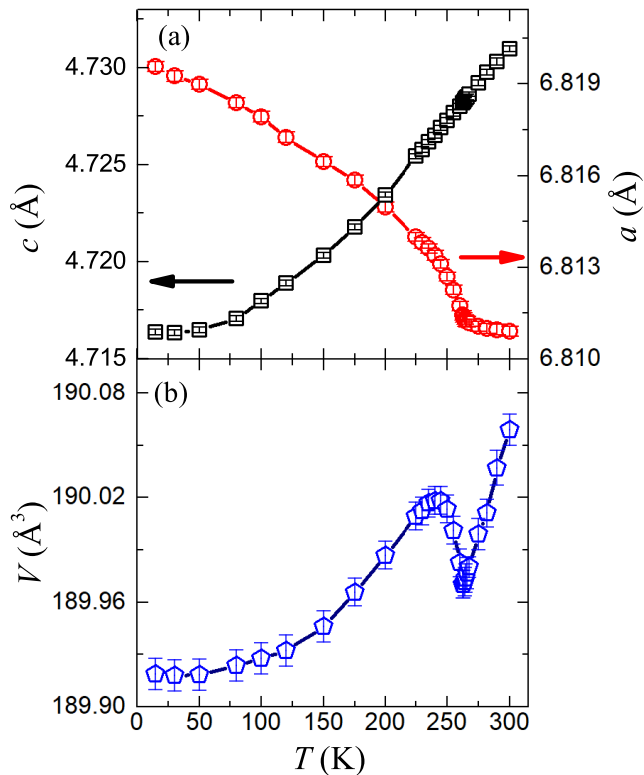


FIG. 2. The variation of lattice parameters (a) a and c and (b) unit cell volume V with temperature, obtained from the Rietveld refinement.

are displayed in Fig. 3 as a function of temperature. It is observed that at the transition temperature, α_a exhibits a large and negative thermal expansion (NTE), whereas α_c shows only a weak and positive anomaly. These results indicate that the transition is accompanied by an anisotropic variation of the unit cell or lattice distortion where it expands rapidly in the ab -plane and contracts weakly along the c -axis. This leads to an overall NTE of the unit cell volume in a wide temperature range 230 K - 265 K. It reaches a minimum value of $\alpha_V \simeq -20 \times 10^{-6} \text{ K}^{-1}$ at the transition temperature, which is comparable to the value reported for large NTE materials such as manganese antiperovskites, itinerant $\text{La}(\text{Fe},\text{Si})_{13}$ compounds etc [5, 6, 8]. As the width of the NTE peak decides the practical use of the compound, one can widen the peak width and tune the transition temperature by introducing disorder in the system through quenching or reduction of particle size and by chemical substitutions [6]. Below the transition, α_V has an almost zero (ZTE) or very small value which remains almost constant ($\sim 2 \times 10^{-6} \text{ K}^{-1}$) with temperature, similar to Invar alloys [3, 29] due to the opposite variation of lattice parameters a and c [see Fig. 2(a)]. The NTE could be related to softening of the phonon modes across the magnetic transition [21, 30]. Moreover, the anisotropic thermal expansion in $\text{Mn}_{1.4}\text{Fe}_{3.6}\text{Si}_3$ across the transi-

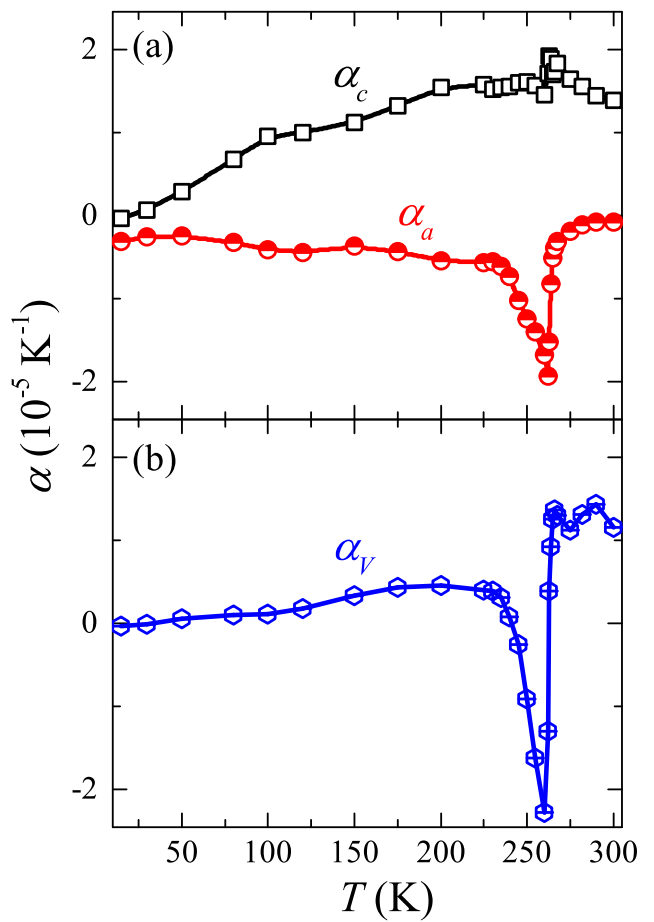


FIG. 3. The variation of thermal expansion co-efficients with temperature for (a) a and c and (b) V .

tion is quite consistent with strong magnetocrystalline anisotropy reported in the parent compound MnFe_4Si_3 , where the easy axis lies in the ab -plane [20, 31]. This indicates that the magnetic transition involves a strong correlation between magnetic and structural degrees of freedom.

For a second-order transition, the change in volumetric thermal expansion coefficient ($\Delta\alpha_V$) at the transition is directly related to the pressure dependence of T_C through the Ehrenfest relation

$$\frac{dT_C}{dP} = \frac{\Delta\alpha_V V_{\text{mol}} T_C}{\Delta C_P}, \text{ near } P = 0. \quad (1)$$

Here, ΔC_P is the change in heat capacity at constant pressure at T_C and V_{mol} is the molar volume. From Eq. (1), one can estimate the variation of T_C with pressure for known values of ΔC_P and $\Delta\alpha_V$. Unfortunately, we don't have C_P data of our compound for doing such an analysis. Nevertheless, the observed negative value of $\Delta\alpha_V$ implies negative $\frac{dT_C}{dP}$, where the transition shifts to lower temperatures with increasing external pressure. Interestingly, this finding is consistent with the pressure

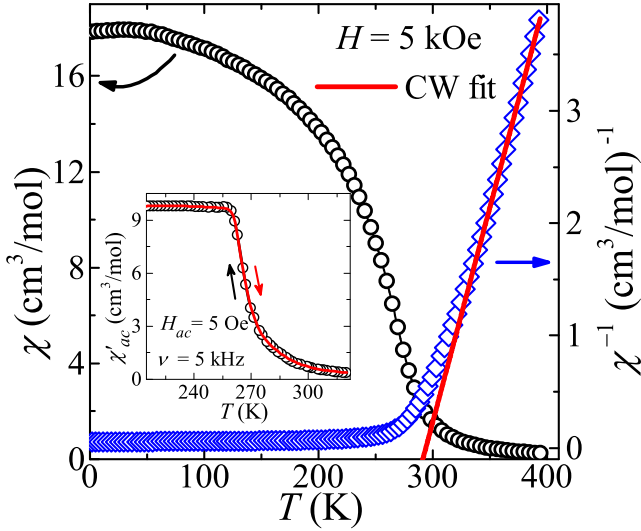


FIG. 4. Temperature dependent magnetic susceptibility $\chi(T)$ and its inverse $\chi^{-1}(T)$ measured in a magnetic field of 5 kOe. Inset: $\chi'_{ac}(T)$ measured during cooling and warming.

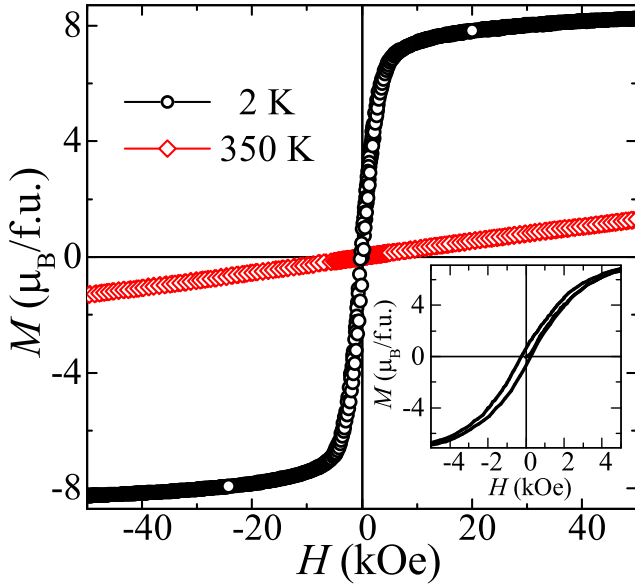


FIG. 5. Isothermal magnetization $[M(H)]$ measured at $T = 350$ K and 2 K. Inset: the $M(H)$ curve $T = 2$ K is magnified in the low field regime to highlight the hysteresis.

dependent study on MnFe_4Si_3 , where $\frac{dT_C}{dP} = -15$ K/GPa is observed [32].

B. Magnetization

Temperature dependent dc -magnetic susceptibility $[\chi(T)]$ and its inverse $[\chi^{-1}(T)]$ for $\text{Mn}_{1.4}\text{Fe}_{3.6}\text{Si}_3$ mea-

sured in an applied field of $H = 5$ kOe are plotted on the left and right y -axes, respectively in Fig. 4. With decrease in temperature, $\chi(T)$ exhibits a sharp raise below 300 K corresponding to the onset of PM to FM transition. The real part of ac -susceptibility $[\chi'_{ac}(T)]$ measured in an ac field of $H_{ac} = 5$ Oe and frequency $\nu = 5$ kHz during cooling and warming is shown in the inset of Fig. 4. No thermal hysteresis is observed around the transition, indicating second order nature of the transition. To estimate the magnetic parameters, the high temperature part of $\chi^{-1}(T)$ is fitted using Curie-Weiss law, $\chi(T) = C/(T - \Theta_{CW})$. Here, C is Curie constant and Θ_{CW} is the paramagnetic Curie temperature. A linear fit ($T \geq 350$ K) yields $\Theta_{CW} \simeq 291.4$ K and effective paramagnetic moment $\mu_{\text{eff}} \simeq 2.31\mu_B$ per transition metal atom using $C = N_A\mu_B^2\mu_{\text{eff}}^2/3k_B$, where N_A is the Avogadro number. These parameters are consistent with the previous report [26].

Figure 5 shows the isothermal magnetization $[M(H)]$ measured at $T = 350$ K and 2 K. The straight line behavior of $M(H)$ curve without any saturation at 350 K represents the typical PM state. On the other hand, the $M(H)$ curve at 2 K shows a sharp increase at low fields with a weak hysteresis and a small coercive field of $H_{\text{cor}} \simeq 250$ Oe, typically expected for a soft ferromagnet. At high fields, magnetization saturates and the value of saturation moment per transition metal atom is estimated to be $\mu_S \simeq 1.61\mu_B$ from the y -intercept of the linear fit to the Arrott plot (M^2 vs H/M) in the high field regime. It is interesting to note that the value of μ_{eff} is relatively larger than μ_S which is a possible indication of the itinerant character of 3d electrons in $\text{Mn}_{1.4}\text{Fe}_{3.6}\text{Si}_3$. Therefore, we calculated the Rhodes-Wohlfarth ratio ($\text{RWR} = q_c/q_s$) where q_c and q_s are the number of magnetic carriers per atom deduced from μ_{eff} and low temperature saturation moment μ_S , respectively [33]. RWR is typically used to distinguish between the localized and itinerant characters of a ferromagnet [34, 35]. In the case of a localized ferromagnet, RWR should be close to 1, whereas for an itinerant ferromagnet the saturation magnetization is less than the fully polarized moment producing $\text{RWR} > 1$. For $\text{Mn}_{1.4}\text{Fe}_{3.6}\text{Si}_3$, we calculated $q_c = 1.52$ from μ_{eff} using the relation $\mu_{\text{eff}}^2 = q_c(q_c + 2)$ and $q_s = 0.89$ from μ_S at 2 K using $\mu_S^2 = q_s(q_s + 2)$. Thus, the obtained $\text{RWR} = 1.71 > 1$ indicates itinerant character of the ferromagnet $\text{Mn}_{1.4}\text{Fe}_{3.6}\text{Si}_3$.

C. Magnetocaloric Effect and Critical Behaviour

The MCE for the polycrystalline $\text{Mn}_{1.4}\text{Fe}_{3.6}\text{Si}_3$ is obtained in term of magnetic entropy change (ΔS_m). ΔS_m is calculated from the magnetic isotherms measured between 150 - 350 K using the standard expression derived from the Maxwell relation:

$$\Delta S_m = \int_{H_i}^{H_f} \frac{dM}{dT} dH. \quad (2)$$

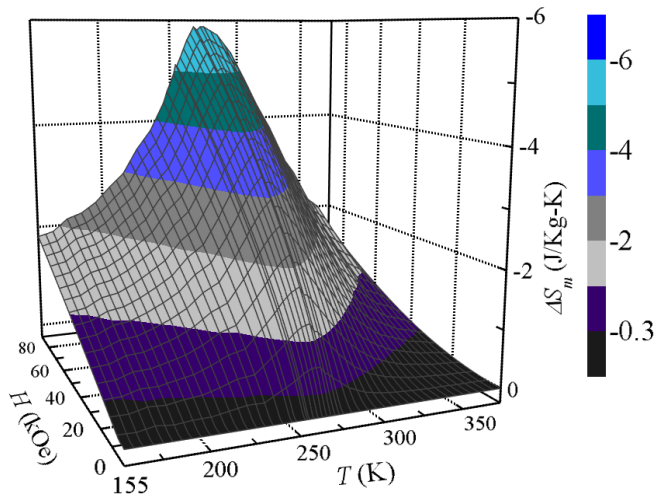


FIG. 6. Temperature and magnetic field dependent 3D plots of magnetic entropy change (ΔS_m).

The results of our ΔS_m calculation are presented in Fig. 6 as a function of magnetic field and temperature in the 3D-plot. The ΔS_m curves exhibit a gradual variation with temperature and show a maximum at T_C . The shape of ΔS_m plots indicate a typical second order transition at T_C [36, 37]. The maximum value of $\Delta S_m \simeq -6$ J/kg-K is achieved for a field change of 90 kOe. The relative cooling power ($RCP = |\Delta S_m^{\text{pk}} \times \delta T_{\text{FWHM}}|$) is another important parameter for a magnetic refrigeration material and it corresponds to the amount of heat transferred between the source and sink of a refrigerator. Here, ΔS_m^{pk} and δT_{FWHM} are the maximum value of ΔS_m at the peak position and the full width at half maximum of the $\Delta S_m(T)$ curve, respectively. ΔS_m^{pk} and δT_{FWHM} as a function of H , obtained from Fig. 6 are plotted in Fig. S7(a) of the Supplementary Material. The RCP value estimated for each $\Delta S_m(T)$ curve at different magnetic fields is shown in Fig. S7(b) of the Supplementary Material. It is found to increase with field and reaches a maximum value ~ 709 J/Kg for 90 kOe. These values of ΔS_m and RCP are comparable to the values reported for other compositions in $\text{Mn}_{1+x}\text{Fe}_{4-x}\text{Si}_3$ series [26].

The critical exponents that reflect the universality class of the spin system are determined using the magnetic isotherms and MCE data following the procedure reported in Ref. [26]. Please see the Supplementary Material for details of the critical analysis. In Table I, the critical exponents obtained from different techniques for compositions $x = 0.0, 0.2,$ and 0.4 are listed along with the theoretically expected values for different universality classes. Adopting the iterative method with the modified Arrott plot (MAP) and from magnetic isotherm at T_C , the critical exponents are obtained to be $\beta = 0.304$, $\gamma = 1.4445$, and $\delta \simeq 5.71$ with $T_C \simeq 254$ K. These values are further confirmed from the Kouvel-Fisher (KF) method and Widom scaling relation. These values of ex-

ponents are identical to the other compositions in the $\text{Mn}_{1+x}\text{Fe}_{4-x}\text{Si}_3$ series and do not fall under any conventional universality class [26]. Similar unconventional critical behavior has also been observed in various ferromagnets [39–44].

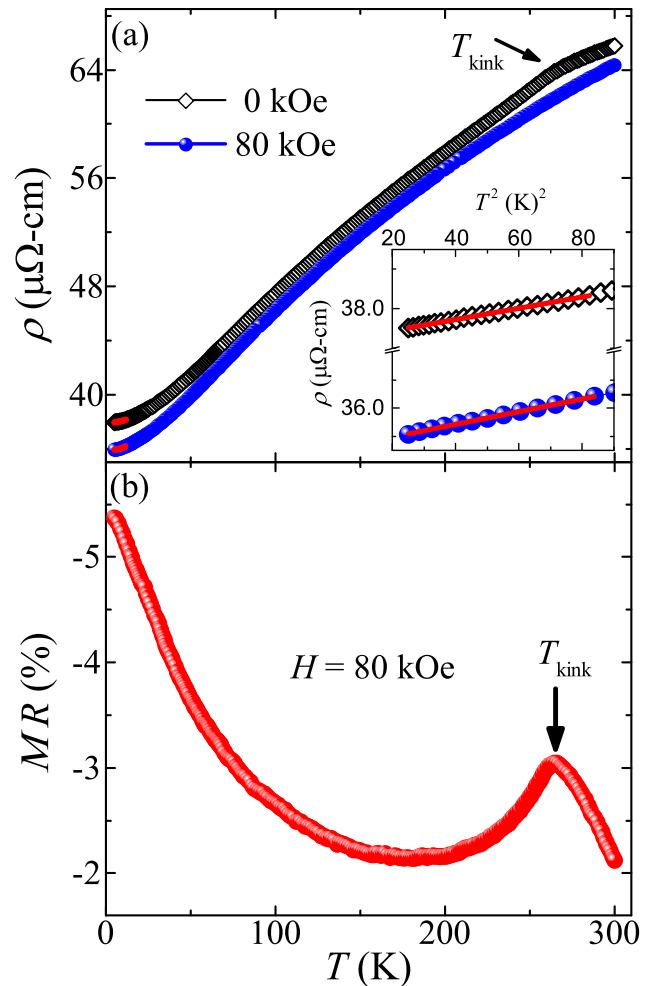


FIG. 7. (a) Temperature dependent resistivity [$\rho(T)$] in zero field and 80 kOe. Inset: ρ vs T^2 at low temperatures highlighting the fit using Eq. (3). (b) Magnetoresistance [$MR(\%)$] as a function of temperature in 80 kOe.

Typically, in a short-range model, the exchange interaction $J(r)$ decays rapidly with distance r as $J(r) \sim e^{-r/\xi}$. On the other hand, for long-range interactions, the exchange interaction in d -dimension should decay following $J(r) \sim r^{-(d+\sigma)}$ which is valid for the range of exchange interaction ($\sigma < 2$ [45]). The final value of $\sigma = 1.41$ was obtained by examining the renormalization theory for the critical exponents choosing lattice dimensionality $d = 2$ and spin dimensionality $n = 1$ for $\gamma = 1.445$. The accuracy of these exponents are also tested by recalculating the other critical exponents (see the Supplementary Material). Thus, $d = 2$, $n = 1$, and $\sigma < 2$ reflect that the system belongs to a 2D Ising

TABLE I. The critical exponents (β , γ , δ , and n) and T_C of $\text{Mn}_{1+x}\text{Fe}_{4-x}\text{Si}_3$ obtained from the modified Arrott plot (MAP), Kouvel-Fisher (KF) plot, critical isotherm (CI), and magnetocaloric effect (MCE)/relative cooling power (RCP) analysis across the PM-FM transition. For comparison, critical exponents corresponding to different theoretical models are also listed.

System	Method	β	γ	δ	n	T_C	Ref.
$x = 0.4$	MAP	0.304(3)	1.445(4)	5.75(4)	0.602	254.0(2)	This work
	KF	0.301(4)	1.441(4)	5.78(7)	0.60	253.9(1)	
	CI	–	–	5.71(6)	–	254	
	MCE/RCP	–	–	5.69(7)	0.601	254	
$x = 0.2$	MAP	0.304(3)	1.445(4)	5.75(4)	0.602	278.17(3)	[26]
	KF	0.301(1)	1.45(1)	5.77(4)	0.600	278.1(1)	
	CI	–	–	5.64(3)	–	278	
	MCE/RCP	–	–	5.73(13)	0.607	278	
$x = 0.0$	MAP	0.308(3)	1.448(5)	5.641(4)	0.606	309.60(2)	[26]
	KF	0.303(4)	1.451(4)	5.77(7)	0.603	309.7(1)	
	CI	–	–	5.644(9)	–	309.6	
	MCE/RCP	–	–	5.70(7)	0.604	309.6	
Mean-field model	Theory	0.5	1.0	3.0			[38]
3D-Heisenberg model	Theory	0.365	1.386	4.80			[38]
3D-Ising model	Theory	0.325	1.241	4.82			[38]
3D-XY	Theory	0.345	1.316	4.81			[38]

universality class with a long-range exchange interaction decaying as $J(r) \sim r^{-3.41}$. Our findings of the critical exponents are similar to that reported for ferromagnets Y_2Ni_7 and URhAl where the quasi-2D Ising character with long-range interactions is explained in term of strong anisotropy in the ab -plane and itinerant character of the magnetism [42, 43]. Thus, the observed itinerant character of $3d$ electrons and strong anisotropy in the ab -plane at the transition temperature are the main sources of the quasi-2D Ising behavior with long-range interactions in $\text{Mn}_{1.4}\text{Fe}_{3.6}\text{Si}_3$ and other compounds in the $\text{Mn}_{1+x}\text{Fe}_{4-x}\text{Si}_3$ series.

D. Resistivity and Magnetoresistance

Figure 7(a) depicts the temperature dependent resistivity $[\rho(T)]$ in zero magnetic field and 80 kOe in the temperature range 4 K to 310 K. The decrease of ρ with T reflects the metallic character of the compound. In zero field, $\rho(T)$ exhibits a weak anomaly or kink at $T_{\text{kink}} \simeq 264.7$ K which corresponds to the PM-FM transition, similar to other metallic ferromagnets [42, 46, 47]. At low-temperatures, $\rho(T)$ is fitted by

$$\rho = \rho_0 + A T^2. \quad (3)$$

Here, ρ_0 is the residual resistivity and A is the coefficient of T^2 . The inset of Fig. 7(a) presents the linear variation of $\rho(T)$ with T^2 which is a representation of the Fermi-liquid behavior likely due to electron-electron scattering at low temperatures [48, 49]. Both the data sets below

9 K are fitted by Eq. (3) yielding ($\rho_0 \simeq 37.91 \mu\Omega \text{ cm}$, $A \simeq 0.001434 \mu\Omega \text{ cm/K}^2$) and ($\rho_0 \simeq 35.852 \mu\Omega \text{ cm}$, $A \simeq 0.0022 \mu\Omega \text{ cm/K}^2$), in zero field and 80 kOe, respectively. The value of residual resistivity ratio is calculated to be $\text{RRR} = \rho_{300\text{K}}/\rho_0 \simeq 1.83$ in zero field, indicating good quality of the sample. Further, as the magnetic field is applied the residual resistivity ρ_0 is reduced significantly which could be related to the complex magnetic scatterings at low temperatures.

The temperature dependent magnetoresistance $\left[MR(\%) = \frac{\rho(H,T) - \rho(0,T)}{\rho(0,T)} \times 100\right]$ calculated from the resistivity data in zero field and in 80 kOe is presented in Fig. 7(b). The negative MR is observed through out the temperature range (4-300 K) which increases with decreasing temperature, exhibits a broad hump around T_{kink} and then shows a gradual increase at low temperatures. A large and negative value of $MR \simeq -3\%$ at the transition temperature can be attributed to the suppression of spin disorder by the application of magnetic field [50]. The isothermal MR as a function of magnetic field measured near the transition ($T = 267.5$ K) and at room temperature ($T = 300$ K) is shown in Fig. 8(a). The negative MR increases with field and its value at $H = 80$ kOe matches with $MR(T)$ data in Fig. 7(b).

The isothermal MR data are fitted by power law $MR(H) \propto H^n$. At $T = 300$ K, it exhibits almost a linear behavior with an exponent $n \simeq 1.1$, whereas a reduced exponent $n \simeq 0.66$ is obtained for $T = 267.5$ K. Interestingly, these values of n are identical to the values obtained from the fit of MCE data by $\Delta S_m(H) \propto H^n$, as shown in Fig. 8(b) and also consistent with the n vs

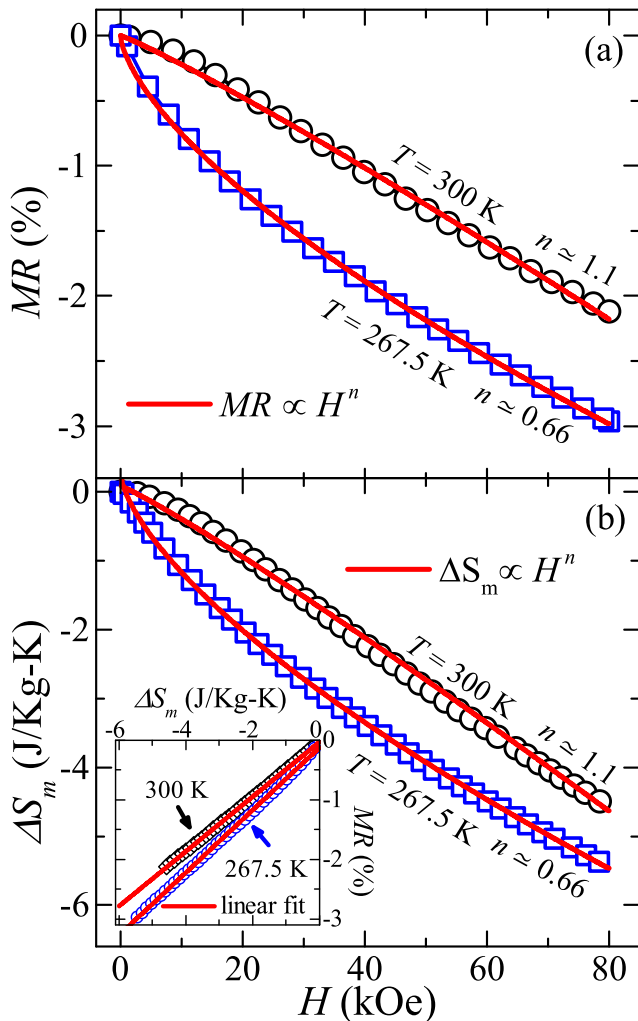


FIG. 8. (a) Magnetic field dependent $MR(\%)$ at $T = 300$ K and 267.5 K. (b) ΔS_m vs H at $T = 300$ K and 267.5 K and the solid lines are the fits. Inset: Linear variation of $MR(\%)$ with ΔS_m .

T and H plot in Fig. S6 (Supplementary Material). Further, MR as a function of ΔS_m with H as an explicit parameter [inset of Fig. 8(b)] exhibits a linear behavior for both the temperatures. The identical field dependence of MR and MCE isotherms indicates that both the quantities are correlated and have same origin. This

also suggests the itinerant character of $3d$ electrons in the studied compound. The identical behaviour of MR and MCE across the magnetic transition is previously reported in different intermetallic compounds with itinerant character [46, 51–55].

IV. CONCLUSION

The structural, magnetic, and electronic properties of $Mn_{1.4}Fe_{3.6}Si_3$ are investigated in detail by means of the temperature dependent powder XRD, magnetization, MCE , and MR measurements. An anisotropic structural distortion is observed across the magnetic transition, where the lattice expands in the ab -plane and contracts slightly along the c -axis. This results in a large negative volume thermal expansion ($\alpha_V \sim -20 \times 10^{-6} \text{ K}^{-1}$) across the transition temperature. The critical analysis of magnetization and MCE data supports the second order nature of the phase transition which can be described in the framework of a quasi-2D Ising model with long-range magnetic interactions. The effective 2D character of the magnetic interactions originates from strong in-plane anisotropy across the transition while the itinerant or delocalized character of the $3d$ electrons is responsible for the long-range magnetic interactions in the $Mn_{1+x}Fe_{4-x}Si_3$ series.

V. SUPPLEMENTARY MATERIAL

See the supplementary material for the critical analysis of magnetization and magnetocaloric effect data.

VI. ACKNOWLEDGMENTS

We acknowledge BRNS, India for financial support bearing sanction Grant No.37(3)/14/26/2017. VS was supported by IISER Thiruvananthapuram postdoctoral program.

VII. DATA AVAILABILITY

The data that support the findings of this study are available within the article [and its Supplementary Material].

- [1] K. Takenaka, Negative thermal expansion materials: technological key for control of thermal expansion, *Sci. Technol. Adv. Mater.* **13**, 013001 (2012).
- [2] T. A. Mary, J. S. O. Evans, T. Vogt, and A. W. Sleight, Negative thermal expansion from 0.3 to 1050 Kelvin in ZrW_2O_8 , *Science* **272**, 90 (1996).

- [3] C. E. Guillaume, Recherches sur les aciers au nickel. dilatations aux temperatures elevees; resistance électrique, *C. R. Acad. Sci.* **125**, 235 (1897).
- [4] M. van Schilfgaarde, I. A. Abrikosov, and B. Johansson, Origin of the Invar effect in iron–nickel alloys, *Nature* **400**, 46 (1999).

- [5] K. Takenaka and H. Takagi, Zero thermal expansion in a pure-form antiperovskite manganese nitride, *App. Phys. Lett.* **94**, 131904 (2009).
- [6] X. Song, Z. Sun, Q. Huang, M. Rettenmayr, X. Liu, M. Seyring, G. Li, G. Rao, and F. Yin, Adjustable zero thermal expansion in antiperovskite manganese nitride, *Adv. Mater.* **23**, 4690 (2011).
- [7] J. Chen, K. Nittala, J. S. Forrester, J. L. Jones, J. Deng, R. Yu, and X. Xing, The role of spontaneous polarization in the negative thermal expansion of tetragonal PbTiO_3 -based compounds, *J. Am. Chem. Soc.* **133**, 11114 (2011).
- [8] R. Huang, Y. Liu, W. Fan, J. Tan, F. Xiao, L. Qian, and L. Li, Giant negative thermal expansion in NaZn_{13} -type $\text{La}(\text{Fe}, \text{Si}, \text{Co})_{13}$ compounds, *J. Am. Chem. Soc.* **135**, 11469 (2013).
- [9] A. L. Goodwin, M. Calleja, M. J. Conterio, M. T. Dove, J. S. O. Evans, D. A. Keen, L. Peters, and M. G. Tucker, Colossal positive and negative thermal expansion in the framework material $\text{Ag}_3[\text{Co}(\text{CN})_6]$, *Science* **319**, 794 (2008).
- [10] Y. Song, X. Chen, V. Dabade, T. W. Shield, and R. D. James, Enhanced reversibility and unusual microstructure of a phase-transforming material, *Nature* **502**, 85 (2013).
- [11] F.-x. Hu, B.-g. Shen, J.-r. Sun, Z.-h. Cheng, G.-h. Rao, and X.-x. Zhang, Influence of negative lattice expansion and metamagnetic transition on magnetic entropy change in the compound $\text{LaFe}_{11.6}\text{Si}_{1.6}$, *App. Phys. Lett.* **78**, 3675 (2001).
- [12] B. K. Greve, K. L. Martin, P. L. Lee, P. J. Chupas, K. W. Chapman, and A. P. Wilkinson, Pronounced negative thermal expansion from a simple structure: Cubic ScF_3 , *J. Am. Chem. Soc.* **132**, 15496 (2010).
- [13] J. Chen, L. Hu, J. Deng, and X. Xing, Negative thermal expansion in functional materials: controllable thermal expansion by chemical modifications, *Chem. Soc. Rev.* **44**, 3522 (2015).
- [14] Y. Song, J. Chen, X. Liu, C. Wang, J. Zhang, H. Liu, H. Zhu, L. Hu, K. Lin, S. Zhang, and X. Xing, Zero thermal expansion in magnetic and metallic $\text{Tb}(\text{Co}, \text{Fe})_2$ intermetallic compounds, *J. Am. Chem. Soc.* **140**, 602 (2018).
- [15] Y. Song, Y. Qiao, Q. Huang, C. Wang, X. Liu, Q. Li, J. Chen, and X. Xing, Opposite thermal expansion in isostructural noncollinear antiferromagnetic compounds of Mn_3A ($\text{A} = \text{Ge}$ and Sn), *Chem. Mater.* **30**, 6236 (2018).
- [16] P. Álvarez-Alonso, P. Gorria, J. A. Blanco, J. Sánchez-Marcos, G. J. Cuello, I. Puente-Orench, J. A. Rodríguez-Velamazán, G. Garbarino, I. de Pedro, J. R. Fernández, and J. L. Sánchez Llamazares, Magnetovolume and magnetocaloric effects in $\text{Er}_2\text{Fe}_{17}$, *Phys. Rev. B* **86**, 184411 (2012).
- [17] B. Li, X. H. Luo, H. Wang, W. J. Ren, S. Yano, C.-W. Wang, J. S. Gardner, K.-D. Liss, P. Miao, S.-H. Lee, T. Kamiyama, R. Q. Wu, Y. Kawakita, and Z. D. Zhang, Colossal negative thermal expansion induced by magnetic phase competition on frustrated lattices in laves phase compound $(\text{Hf}, \text{Ta})\text{Fe}_2$, *Phys. Rev. B* **93**, 224405 (2016).
- [18] Y. Song, Q. Sun, M. Xu, J. Zhang, Y. Hao, Y. Qiao, S. Zhang, Q. Huang, X. Xing, and J. Chen, Negative thermal expansion in $(\text{Sc}, \text{Ti})\text{Fe}_2$ induced by an unconventional magnetovolume effect, *Mater. Horiz.* **7**, 275 (2020).
- [19] Q. Ren, W. Hutchison, J. Wang, A. Studer, G. Wang, H. Zhou, J. Ma, and S. J. Campbell, Negative thermal expansion of Ni-doped MnCoGe at room-temperature magnetic tuning, *ACS Appl. Mater. Interfaces* **11**, 17531 (2019).
- [20] P. Hering, K. Friese, J. Voigt, J. Persson, N. Aliouane, A. Grzechnik, A. Senyshyn, and T. Brückel, Structure, magnetism, and the magnetocaloric effect of MnFe_4Si_3 single crystals and powder samples, *Chem. Mater.* **27**, 7128 (2015).
- [21] M. Herlitschke, B. Klobes, I. Sergueev, P. Hering, J. Perßon, and R. P. Hermann, Elasticity and magnetocaloric effect in MnFe_4Si_3 , *Phys. Rev. B* **93**, 094304 (2016).
- [22] V. Franco, J. Y. Law, A. Conde, V. Brabander, D. Y. Karpenkov, I. Radulov, K. Skokov, and O. Gutfleisch, Predicting the tricritical point composition of a series of LaFeSi magnetocaloric alloys via universal scaling, *J. Phys. D: Appl. Phys.* **50**, 414004 (2017).
- [23] A. Fujita, S. Fujieda, Y. Hasegawa, and K. Fukamichi, Itinerant-electron metamagnetic transition and large magnetocaloric effects in $\text{La}(\text{Fe}_x\text{Si}_{1-x})_{13}$ compounds and their hydrides, *Phys. Rev. B* **67**, 104416 (2003).
- [24] N. H. Dung, L. Zhang, Z. Q. Ou, and E. Brück, From first-order magneto-elastic to magneto-structural transition in $(\text{Mn}, \text{Fe})_{1.95}\text{P}_{0.50}\text{Si}_{0.50}$ compounds, *App. Phys. Lett.* **99**, 092511 (2011).
- [25] D. Zhao, T. Castán, A. Planes, Z. Li, W. Sun, and J. Liu, Enhanced caloric effect induced by magnetoelastic coupling in NiMnGaCu heusler alloys: Experimental study and theoretical analysis, *Phys. Rev. B* **96**, 224105 (2017).
- [26] V. Singh, P. Bag, R. Rawat, and R. Nath, Critical behavior and magnetocaloric effect across the magnetic transition in $\text{Mn}_{1+x}\text{Fe}_{4-x}\text{Si}_3$, *Sci. Rep.* **10**, 6981 (2020).
- [27] J. Rodríguez-Carvajal, Recent advances in magnetic structure determination by neutron powder diffraction, *Physica B* **192**, 55 (1993).
- [28] S. N. Kaul and S. Srinath, Gadolinium: A helical antiferromagnet or a collinear ferromagnet, *Phys. Rev. B* **62**, 1114 (2000).
- [29] E. F. Wasserman, Chapter 3 Invar: Moment-volume instabilities in transition metals and alloys, in *Handbook of Ferromagnetic Materials*, Vol. 5 (Elsevier, 1990) pp. 237–322.
- [30] M. E. Gruner, W. Keune, B. Roldan Cuenya, C. Weis, J. Landers, S. I. Makarov, D. Klar, M. Y. Hu, E. E. Alp, J. Zhao, M. Krautz, O. Gutfleisch, and H. Wende, Element-resolved thermodynamics of magnetocaloric $\text{LaFe}_{13-x}\text{Si}_x$, *Phys. Rev. Lett.* **114**, 057202 (2015).
- [31] N. Biniskos, S. Raymond, K. Schmalzl, A. Schneidewind, J. Voigt, R. Georgii, P. Hering, J. Persson, K. Friese, and T. Brückel, Spin dynamics of the magnetocaloric compound MnFe_4Si_3 , *Phys. Rev. B* **96**, 104407 (2017).
- [32] E. Andreas, A. Grzechnik, L. Caron, Y. Cheng, J. Wilden, H. Deng, V. Hutanu, M. Meven, M. Hanfland, K. Glazyrin, P. Hering, M. G. Herrmann, M. A. Haddouch, and K. Friese, Magnetocaloric Mn_5Si_3 and MnFe_4Si_3 at variable pressure and temperature, *Mater. Res. Express* **6**, 096118 (2019).

- [33] P. Rhodes, E. P. Wohlfarth, and H. Jones, The effective curie-weiss constant of ferromagnetic metals and alloys, *Proc. Roy. Soc. (London)* **273**, 247 (1963).
- [34] E. P. Wohlfarth, Magnetic properties of crystalline and amorphous alloys: A systematic discussion based on the rhodes-wohlfarth plot, *J. Magn. Magn. Mater.* **7**, 113 (1978).
- [35] A. K. Pramanik and A. Banerjee, Critical behavior at paramagnetic to ferromagnetic phase transition in $\text{Pr}_{0.5}\text{Sr}_{0.5}\text{MnO}_3$: A bulk magnetization study, *Phys. Rev. B* **79**, 214426 (2009).
- [36] J. Y. Law, V. Franco, L. M. Moreno-Ramírez, A. Conde, D. Y. Karpenkov, I. Radulov, K. P. Skokov, and O. Gutfleisch, A quantitative criterion for determining the order of magnetic phase transitions using the magnetocaloric effect, *Nat. Commun.* **9**, 2680 (2018).
- [37] S. S. Islam, V. Singh, K. Somesh, P. K. Mukharjee, A. Jain, S. M. Yusuf, and R. Nath, Unconventional superparamagnetic behavior in the modified cubic spinel compound $\text{LiNi}_{0.5}\text{Mn}_{1.5}\text{O}_4$, *Phys. Rev. B* **102**, 134433 (2020).
- [38] S. N. Kaul, Static critical phenomena in ferromagnets with quenched disorder, *J. Magn. Magn. Mater.* **53**, 5 (1985).
- [39] R. Reisser, M. Fähnle, and H. Kronmüller, Magnetic phase transitions in FeNiBSi alloys, *Journal of Magnetism and Magnetic Materials* **97**, 83 (1991).
- [40] J.-G. Cheng, Y. Sui, J.-S. Zhou, J. B. Goodenough, and W. H. Su, Transition from orbital liquid to jahn-teller insulator in orthorhombic perovskites RTiO_3 , *Phys. Rev. Lett.* **101**, 087205 (2008).
- [41] J.-S. Zhou, K. Matsubayashi, Y. Uwatoko, C.-Q. Jin, J.-G. Cheng, J. B. Goodenough, Q. Q. Liu, T. Katsura, A. Shatskiy, and E. Ito, Critical behavior of the ferromagnetic perovskite BaRuO_3 , *Phys. Rev. Lett.* **101**, 077206 (2008).
- [42] A. Bhattacharyya, D. Jain, V. Ganesan, S. Giri, and S. Majumdar, Investigation of weak itinerant ferromagnetism and critical behavior of Y_2Ni_7 , *Phys. Rev. B* **84**, 184414 (2011).
- [43] N. Tateiwa, J. Pospíšil, Y. Haga, and E. Yamamoto, Critical behavior of magnetization in URhAl: Quasi-two-dimensional ising system with long-range interactions, *Phys. Rev. B* **97**, 064423 (2018).
- [44] N. Su, F. Li, Y. Jiao, Z. Liu, J. Sun, B. Wang, Y. Sui, H. Zhou, G. Chen, and J. Cheng, Asymmetric ferromagnetic criticality in pyrochlore ferromagnet $\text{Lu}_2\text{V}_2\text{O}_7$, *Sci. Bull.* **64**, 1222 (2019).
- [45] M. E. Fisher, S. K. Ma, and B. G. Nickel, Critical exponents for long-range interactions, *Phys. Rev. Lett.* **29**, 917 (1972).
- [46] S. S. Samatham and V. Ganesan, Critical behavior, universal magnetocaloric, and magnetoresistance scaling of MnSi, *Phys. Rev. B* **95**, 115118 (2017).
- [47] E. A. Yelland, S. J. C. Yates, O. Taylor, A. Griffiths, S. M. Hayden, and A. Carrington, Ferromagnetic properties of ZrZn_2 , *Phys. Rev. B* **72**, 184436 (2005).
- [48] H. v. Löhneysen, A. Rosch, M. Vojta, and P. Wölfle, Fermi-liquid instabilities at magnetic quantum phase transitions, *Rev. Mod. Phys.* **79**, 1015 (2007).
- [49] G. R. Stewart, Non-fermi-liquid behavior in *d*- and *f*-electron metals, *Rev. Mod. Phys.* **73**, 797 (2001).
- [50] H. Yamada and S. Takada, Negative Magnetoresistance of Ferromagnetic Metals due to Spin Fluctuations, *Prog. Theor. Phys.* **48**, 1828 (1972).
- [51] V. Singh, R. Kumar, P. Bag, R. Rawat, and P. Kushwaha, Magnetocaloric effect and magnetoresistance correlation in Ge-doped Mn_2Sb , *Mater. Res. Express* **1**, 046101 (2014).
- [52] R. Rawat and I. Das, The similar dependence of the magnetocaloric effect and magnetoresistance in TmCu and TmAg compounds and its implications, *J. Phys.: Condens. Matter* **13**, L379 (2001).
- [53] I. Das and R. Rawat, A study of magnetocaloric effect in PrCo_2Si_2 to understand contributions to magnetoresistance, *Solid State Commun.* **115**, 207 (2000).
- [54] J. C. P. Campoy, E. J. R. Plaza, A. A. Coelho, and S. Gama, Magnetoresistivity as a probe to the field-induced change of magnetic entropy in RAl_2 compounds ($R = \text{Pr, Nd, Tb, Dy, Ho, Er}$), *Phys. Rev. B* **74**, 134410 (2006).
- [55] S. Gupta, R. Rawat, and K. G. Suresh, Large field-induced magnetocaloric effect and magnetoresistance in ErNiSi, *Appl. Phys. Lett.* **105**, 012403 (2014).
-

Supplementary Material for ”Negative thermal expansion and itinerant ferromagnetism in $\text{Mn}_{1.4}\text{Fe}_{3.6}\text{Si}_3$ ”

S-I. CRITICAL BEHAVIOUR

A. Critical analysis of magnetization

The critical behaviour analysis across a ferromagnetic transition temperature (T_C) provides vital information about the phase transition and the exchange interaction. The critical behavior is characterized by a set of exponents (β , γ , and δ) and the universality class of a magnetic system is typically decided on the basis of critical exponent values *i.e.* mean-field model, Heisenberg model, Ising model, and 3D-XY model etc.[S1]. These critical exponents are associated with spontaneous magnetization (M_S), zero field inverse susceptibility (χ_0^{-1}), and critical isotherm at T_C through the following expressions.[S2]

$$M_S(T) = M_0(-\epsilon)^\beta, \text{ for } \epsilon < 0, T < T_C, \quad (\text{S1})$$

$$\chi_0^{-1}(T) = \Gamma(\epsilon)^\gamma, \text{ for } \epsilon > 0, T > T_C, \quad (\text{S2})$$

and

$$M(H) = X(H)^{1/\delta}, \text{ for } \epsilon = 0, T = T_C. \quad (\text{S3})$$

Here, $\epsilon = \frac{T - T_C}{T_C}$ is the reduced temperature, H is applied field, and M_0 , Γ , and X are the critical coefficients. These critical exponents are universal and related to each other through the following scaling laws [S3]

$$\alpha + 2\beta + \gamma = 2 \quad (\text{S4})$$

and

$$\delta = 1 + \frac{\gamma}{\beta}. \quad (\text{S5})$$

Apart from these relations, the exponents should also satisfy the scaling equation of state which relates magnetization M with H and T just above and below the T_C as

$$M(H, \epsilon) |\epsilon|^{-\beta} = f_\pm(H |\epsilon|^{-(\beta+\gamma)}). \quad (\text{S6})$$

Here, f_+ and f_- are the scaling functions just above and below T_C , respectively. The terms in the left and right hand sides of Eq. (S6) can also be written in terms of reduced magnetization $m = M(H, \epsilon)\epsilon^{-\beta}$ and reduced field $h = H |\epsilon|^{-(\beta+\gamma)}$, respectively. With the appropriate values of β , γ , and T_C , the curves obtained from the implementation of Eq. (S6) will collapse into two separate universal branches: one above and another below T_C . To determine the critical exponents from the magnetic isotherms we have employed the standard procedure. The conventional Arrott plots [M^2 vs H/M][S4] are constructed from the magnetic isotherms $M(H)$ as depicted in Fig. S1(a). The positive slope of Arrott plots indicates a second order transition [S5]. Clearly, the Arrott plots do not constitute parallel and straight lines as anticipated from the classical mean field model ($\beta = 0.5$ and $\gamma = 1.0$). Therefore, using the Arrott-Noakes equation, we employed modified Arrott plot (MAP) [$M^{1/\beta}$ vs $(H/M)^{1/\gamma}$] to further analyze the magnetic isotherms [S6]. For a reliable estimation of critical exponents, we have used the iterative procedure as described in Ref. [S7]. As a starting point, the initial values of exponents are taken to be $\beta = 0.367$ and $\gamma = 1.388$ corresponding to the Heisenberg Model and iterations are performed till a stable set of critical exponents are achieved. The final values of critical exponents are obtained to be $\beta = 0.304$ and $\gamma = 1.4445$ which are used to construct the MAPs. The resultant straight and parallel lines are presented in Fig. S1(b). The linear fits of the final MAPs in the high field regime are extrapolated to $H/M = 0$ and the final temperature dependent saturation magnetization [$M_S(T)$] and zero-field inverse susceptibility [$\chi_0^{-1}(T)$] are obtained from the intercepts in the $M^{1/\beta}$ - and $(H/M)^{1/\gamma}$ -axes, respectively. In Fig. S1(c), $M_S(T)$ and $\chi_0^{-1}(T)$ are fitted by Eq. (S1) and Eq. (S2) which yield the parameters ($\beta \simeq 0.304$ and $T_C \simeq 254$ K) and ($\gamma \simeq 1.445$ and $T_C \simeq 253.9$ K), respectively.

To determine the more accurate values of parameters β , γ , and T_C , we analyzed $M_S(T)$ and $\chi_0^{-1}(T)$, obtained from the MAPs, using the Kouvel-Fisher (KF) method[S8]:

$$\frac{M_S(T)}{dM_S(T)/dT} = \frac{T - T_C}{\beta(T)} \quad (\text{S7})$$

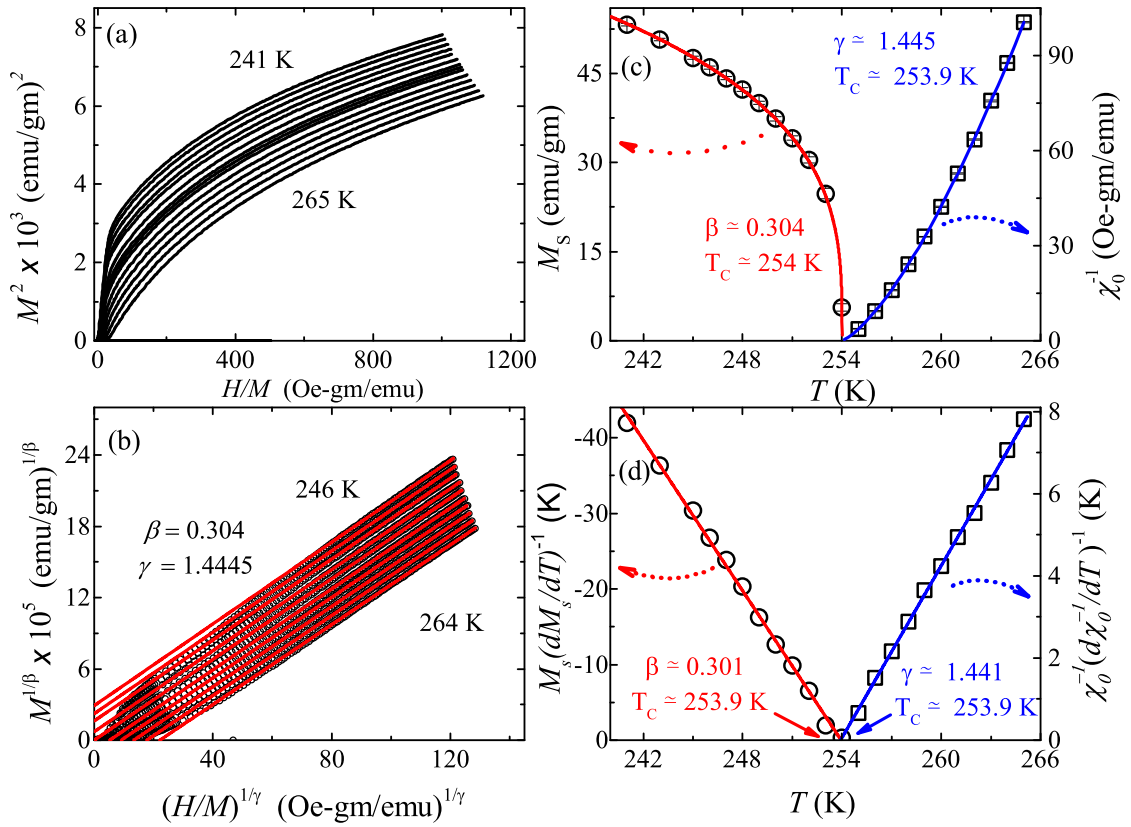


FIG. S1. (a) The Arrott plots: M^2 vs H/M . (b) The modified Arrott plots: $M^{1/\beta}$ vs $H/M^{1/\gamma}$. (c) Spontaneous magnetization (M_S) and zero field inverse susceptibility (χ_0^{-1}) as a function of temperature in the left and right y -axes, respectively (d) The Kouvel-Fisher plot of M_S and χ_0^{-1} as a function of temperature. The solid lines are the linear fits. The solid arrows point to T_C .

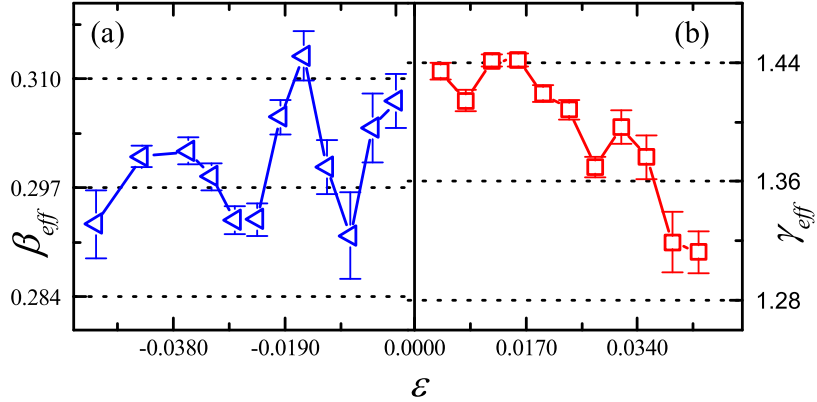


FIG. S2. The variation of effective exponents (a) β_{eff} and (b) γ_{eff} with reduced temperature (ϵ).

and

$$\frac{\chi_0^{-1}(T)}{d\chi_0^{-1}(T)/dT} = \frac{T - T_C}{\gamma(T)}. \quad (\text{S8})$$

Here, the exponents β and γ are temperature dependent and approach the exact values in the limit $T \rightarrow T_C$. Following these equations, we plotted $M_S(T)(dM_S(T)/dT)^{-1}$ and $\chi_0^{-1}(T)(d\chi_0^{-1}(T)/dT)^{-1}$ vs temperature in Fig. S1(d) and the

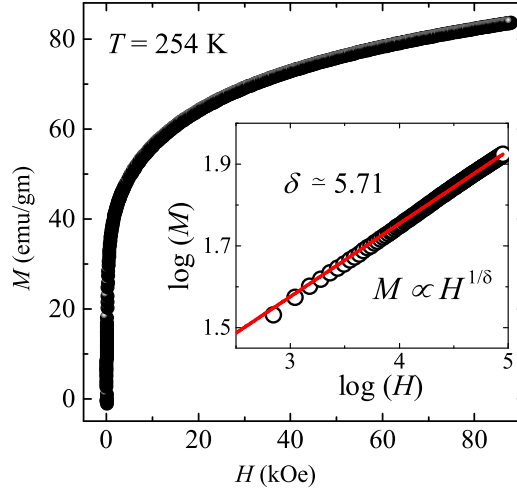


FIG. S3. Isothermal magnetization (M) vs applied field (H) at $T \simeq T_C = 254$ K. Inset: $\log M$ vs $\log H$ plot and the solid line is the linear fit corresponding to Eq. (S3).

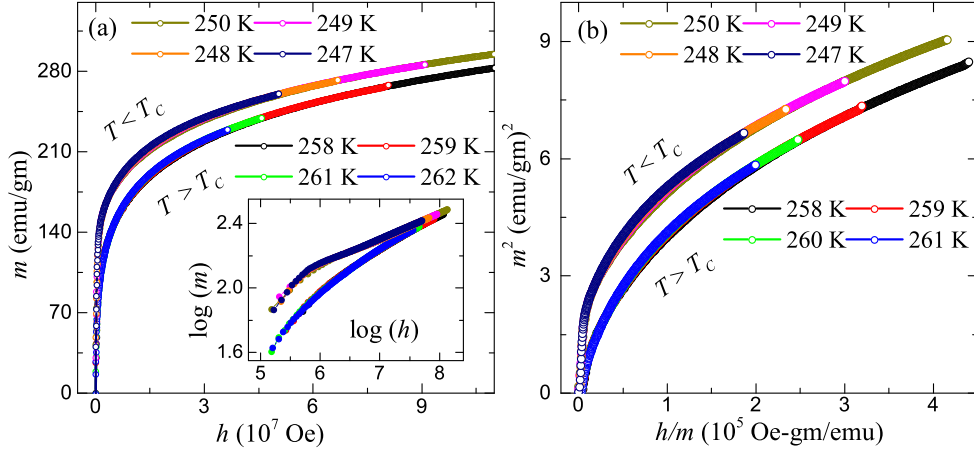


FIG. S4. (a) The reduced magnetization (m) vs reduced field (h) at different temperatures, just above and below T_C . Inset: Log - log plots of the m vs h curves. (b) m^2 vs h/m at the same temperatures around T_C . The renormalized curves in (a) and (b) at different temperatures just above and below T_C are collapsing into two separate branches.

linear fits result $\beta \simeq 0.301$ with $T_C \simeq 253.9$ K and $\gamma \simeq 1.441$ with $T_C \simeq 253.9$ K, respectively. These values of β , γ , and T_C are consistent with the values determined from the MAP analysis.

Clearly, these critical exponents do not follow any conventional universality class.[S9] Therefore, we analyzed the temperature variation of effective exponents (β_{eff} and γ_{eff}) in order to check the presence of any crossover phenomena on approaching T_C which may give rise to these unusual exponents. The effective exponents as a function of ϵ are obtained as:[S7]

$$\beta_{\text{eff}}(\epsilon) = \frac{d[\ln M_S(\epsilon)]}{d(\ln \epsilon)}, \quad \gamma_{\text{eff}}(\epsilon) = \frac{d[\ln \chi_0^{-1}(\epsilon)]}{d(\ln \epsilon)}. \quad (\text{S9})$$

Figures S2(a) and (b) present β_{eff} and γ_{eff} as function of ϵ , respectively. β_{eff} exhibits a nonmonotonic variation within 0.29 to 0.31 and seems to approach the observed $\beta \simeq 0.304$ value in the asymptotic limit ($\epsilon \rightarrow 0$). Similarly, γ_{eff} increases slightly from 1.3 and converges to the observed value $\gamma \simeq 1.44$ for $\epsilon \rightarrow 0$. These observations rule out the presence of any crossover regime near T_C .

The third critical exponent (δ) can be estimated from the Widom relation [Eq. (S5)] using the values of β and γ ,

obtained from MAPs. Using $\beta \simeq 0.304$ and $\gamma \simeq 1.445$ in Eq. (S5), we found $\delta \simeq 5.75$. δ can also be determined independently as per Eq. (S3) using the magnetic isotherm at T_C . Figure S3 contains the critical isotherm at $T_C = 254$ K measured upto $H = 90$ kOe. The inverse slope of the linear fit to the log-log plot (see the inset of Fig. S3) of critical isotherm yields $\delta \simeq 5.71$, which is consistent with the value obtained from the Widom relation.

Finally, the obtained critical exponents should follow the scaling equation of state Eq. (S6) around T_C . The plots of reduced magnetization m as a function of reduced field h using the actual exponents, should form two separate universal branches just above and below T_C . The typical m vs h and m^2 vs h/m plots are depicted in Fig. S4 (a) and (b), respectively. Indeed, the scaled magnetization isotherms of the studied compound follow Eq. (S6) and collapse into two separate branches just above and below T_C . In the inset of Fig. S4(a), we have plotted $\log(m)$ vs $\log(h)$ to show that they exactly follow two branches even in the low field regime. Thus, the above observations unambiguously demonstrate the reliability of the obtained critical exponents and T_C .

B. Scaling and critical analysis of MCE

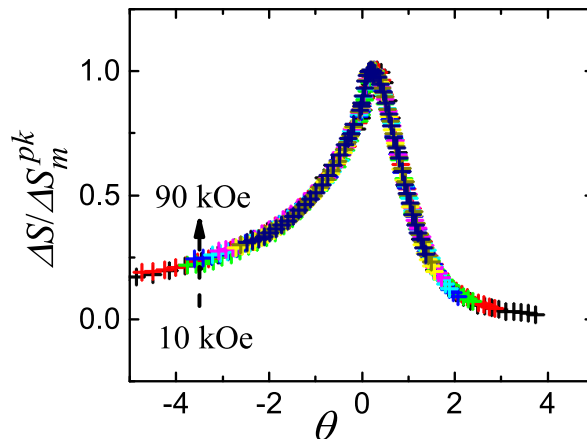


FIG. S5. Normalized magnetic entropy $[\Delta S_m(T)/\Delta S_m^{\text{pk}}]$ vs rescaled temperature θ , obtained using Eq. (S10).

Using the scaling hypothesis Franco *et al*[S10, S11] have shown that the $\Delta S_m(T)$ curves at different magnetic fields should collapse on a single universal curve when the entropy change normalized to its peak value $[\Delta S_m(T)/\Delta S_m^{\text{pk}}]$ is plotted as a function of the rescaled temperature. This universality curve allows us to study the general behavior of $\Delta S_m(T)$ for all applied fields. The rescaled temperature θ can be defined as

$$\theta = \begin{cases} -(T - T_C)/(T_{r1} - T_C), & \text{for } T \leq T_C \\ (T - T_C)/(T_{r2} - T_C), & \text{for } T > T_C, \end{cases} \quad (\text{S10})$$

where T_{r1} and T_{r2} are reference temperatures above and below T_C which should be chosen in such a way that the condition $\Delta S_m(\text{for } T_{r1} < T_C)/\Delta S_m^{\text{pk}} = \Delta S_m(\text{for } T_{r2} > T_C)/\Delta S_m^{\text{pk}} = h$ is satisfied. Here, h is an arbitrary constant which has a value $h < 1$. To construct this phenomenological curve, we used $T_C = 254$ K, obtained from the critical analysis of magnetization and reference temperatures (T_{r1} and T_{r2}) corresponding to $h = 0.5$. As depicted in Fig. S5, a perfect collapse of all the curves is achieved in the full range of θ . This finding is consistent with other compositions of the series $\text{Mn}_{1+x}\text{Fe}_{4-x}\text{Si}_3$ and reflects second order nature of the phase transition.[S9] However, for a first order phase transition these curves do not collapse into a common curve, especially for $\theta < 0$. [S12]

Furthermore, the critical exponents can be extracted from the power law fitting of the field dependent MCE properties (ΔS_m , δT_{FWHM} , and RCP) extracted from Fig. 6 (main text) in the vicinity of T_C . It is demonstrated that magnetic field dependence of ΔS_m can be expressed as:

$$\Delta S_m \text{ or } |\Delta S_m^{\text{pk}}| \propto H^n. \quad (\text{S11})$$

Here the exponent n is temperature and field dependent which can be estimated locally from the following relation[S13]:

$$n(T, H) = \frac{d \ln |\Delta S_m|}{d \ln H}. \quad (\text{S12})$$

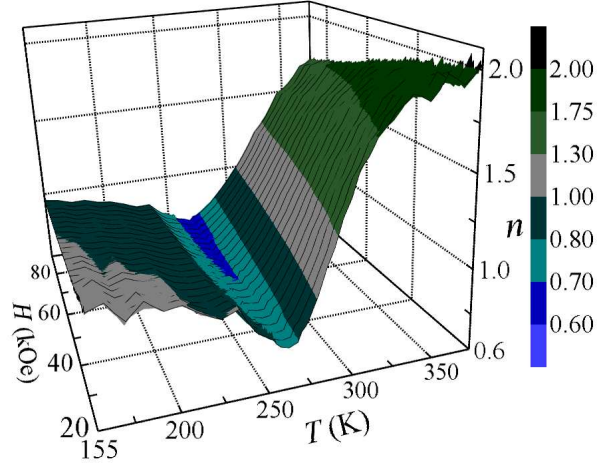


FIG. S6. Temperature and magnetic field dependent 3D plots of exponent n , obtained using Eq. (S12).

In the case of a second order magnetic transition, this relation yields $n = 2$ in the paramagnetic region ($T \gg T_C$) and $n = 1$ for $T \ll T_C$. However, in the critical/asymptotic regime (*i.e.* $T = T_C$ or $\epsilon \rightarrow 0$), n is related to critical exponents β , γ , δ , specific heat exponent (α), and gap exponent (Δ) as[S14]

$$n = 1 + \frac{1}{\delta} \left(1 - \frac{1}{\beta}\right) = 1 + \frac{\beta - 1}{\beta + \gamma} = (1 - \alpha)/\Delta. \quad (\text{S13})$$

Figure S6 presents the 3D plot of exponent n as a function magnetic field and temperature calculated using of Eq. (S12). It approaches value 2 and 1 in the paramagnetic region ($T \gg T_C$) and in the low temperature region ($T \ll T_C$), respectively. $n(T)$ exhibits a minima with $n \simeq 0.601$ at $T = T_C$, typical behavior across a second order transition. Therefore, n is an important exponent which provides information about the critical behavior in the asymptotic regime. Further, we have also estimated n fitting $\Delta S_m^{\text{pk}}(H)$ by Eq. (S11) [see Fig. S7(a)] which yields $n \simeq 0.602$. This value of n is consistent with the values obtained from Fig. S6 at $T = T_C$ and calculated using the β and γ values obtained from the critical analysis of magnetization in Eq. (S13).

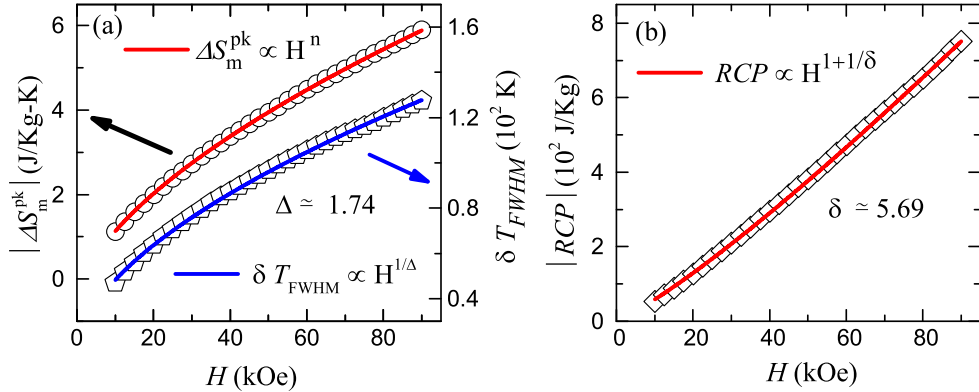


FIG. S7. The magnetic field dependent plot of (a) $|\Delta S_m^{\text{pk}}|$ (left y -axis) and δT_{FWHM} (right y -axis) and (b) relative cooling power (RCP) obtained from Fig. 6 (main text). The solid lines are the fits as described in the text.

Similarly, the other exponents δ and Δ can be directly obtained from the fitting of magnetic field dependent RCP and δT_{FWHM} using the following power laws[S10, S11]

$$\delta T_{\text{FWHM}} \propto H^{1/\Delta}. \quad (\text{S14})$$

and

$$RCP \propto H^{1+1/\delta} \quad (\text{S15})$$

The power law fitting of field dependent δT_{FWHM} and RCP yield the $\Delta \simeq 1.74$ and $\delta \simeq 5.69$ as shown in Fig. S7. Indeed, the obtained gap exponent $\Delta \simeq 1.74$ is consistent with the relation $\Delta = \beta \times \delta = \beta + \gamma$. We have also estimated the specific heat exponent to be $\alpha \simeq -0.045$ using the n and Δ values in Eq. (S13).

The critical exponents obtained from the analysis of magnetization isotherms, ΔS_m , and RCP are consistent with each other, reflecting the reliability of our analysis. The obtained critical exponents from different techniques are tabulated along with the theoretically expected ones in Table I (main text). Clearly, our experimental values of critical exponents do not fall under any of the short-range model universality classes.[S9] In a conventional short-range model, the exchange interaction $J(r)$ decays rapidly with distance r following $J(r) \sim e^{-r/\xi}$. On the other hand, for long-range interactions, the exchange interaction in d -dimension should decay as $J(r) \sim r^{-(d+\sigma)}$ which is valid for the range of exchange interaction (σ) < 2 . [S15] According to renormalization theory, critical exponent γ can be defined as[S15]

$$\begin{aligned} \gamma &= 1 + \frac{4}{d} \left(\frac{n+2}{n+8} \right) \Delta \sigma + \frac{8(n+2)(n-4)}{d^2(n+2)^2} \\ &= \times \left[1 + \frac{2G(\frac{d}{2})(7n+20)}{(n-4)(n+8)} \right] \Delta \sigma^2, \end{aligned} \quad (\text{S16})$$

where $\Delta \sigma = (\sigma - \frac{d}{2})$, $G(\frac{d}{2}) = 3 - \frac{1}{4}(\frac{d}{2})^2$. Using the experimental value of γ for different sets of (d, n) in Eq. (S16) we estimated the corresponding σ values. After various trails with different sets of (d, n) values, a reliable value of $\sigma = 1.41$ was obtained choosing $d = 2$ and $n = 1$ for $\gamma = 1.445$. In order to test the reliability of the σ value, one can recalculate the other critical exponents as $\nu = \gamma/\sigma$, $\eta = 2 - \sigma$, $\alpha = 2 - \nu d$, $\beta = (2 - \alpha - \gamma)/2$, and $\delta = 1 + \gamma/\beta$. [S15, S16] Using $\sigma = 1.41$ in the above relations we estimated $\beta \simeq 0.300$, $\gamma \simeq 1.448$, $\delta \simeq 5.831$, $\nu \simeq 1.02$, $\eta \simeq 0.586$, and $\alpha \simeq -0.0475$ which are consistent with our experimental values, justifying our choice of (d, n) and the estimation of $\sigma = 1.41$. Thus, with $d = 2$, $n = 1$, and $\sigma < 2$ the system belongs to a 2D Ising universality class with a long-range exchange interaction decaying as $J(r) \sim r^{-3.41}$.

-
- [S1] S. N. Kaul, J. Magn. Magn. Mater. **53**, 5 (1985).
[S2] H. E. Stanley, *Introduction to Phase Transitions and Critical Phenomena*, Oxford University Press, (1968) p.336.
[S3] B. Widom, J. Chem. Phys. **43**, 3898 (1965).
[S4] A. Arrott, Phys. Rev. **108**, 1394 (1957).
[S5] B. K. Banerjee, Phys. Lett. **12**, 16 (1964).
[S6] A. Arrott and J. E. Noakes, Phys. Rev. Lett. **19**, 786 (1967).
[S7] A. K. Pramanik and A. Banerjee, Phys. Rev. B **79**, 214426 (2009).
[S8] J. S. Kouvel and M. E. Fisher, Phys. Rev. **136**, A1626 (1964).
[S9] V. Singh, P. Bag, R. Rawat, and R. Nath, Sci. Rep. **10**, 6981 (2020).
[S10] V. Franco, J. S. Blázquez, and A. Conde, Appl. Phys. Lett. **89**, 222512 (2006).
[S11] V. Franco, C. F. Conde, J. S. Blázquez, A. Conde, P. Švec, D. Janičkovič, and L.F. Kiss, J. Appl. Phys. **101**, 093903 (2007).
[S12] C. M. Bonilla, J. Herrero-Albillos, F. Bartolomé, L. M. García, M. Parra-Borderías, and V. Franco, Phys. Rev. B **81**, 224424 (2010).
[S13] T. D. Shen, R. B. Schwarz, J. Y. Coulter, and J. D. Thompson, J. Appl. Phys. **91**, 5240 (2002).
[S14] V. Franco, A. Conde, J. M. Romero-Enrique, and J. S. Blázquez, J. Phys.: Condens. Matter **20**, 285207 (2008).
[S15] M. E. Fisher, S. K. Ma, and B. G. Nickel, Phys. Rev. Lett. **29**, 917 (1972).
[S16] S. F. Fischer, S. N. Kaul, and H. Kronmüller, Phys. Rev. B **65**, 064443 (2002).